Polymer Bulletin (2023) 80:7883–7900
https://doi.org/10.1007/s00289-022-04422-9

ORIGINAL PAPER

Enhanced adsorption of crystal violet from aqueous solution by polyethyleneimine-modified magnetic hydrogel nanocomposites

Tao Wan[1,2] · Yang Jia[2] · Songsong He[2] · Tairan Wang[2] · Jian Wang[2] · Qi Tang[2] · Mingrui Yu[2]

Received: 8 March 2022 / Revised: 25 May 2022 / Accepted: 9 July 2022 /
Published online: 17 August 2022

Abstract

Magnetic hydrogels have huge potential environmental applications in the elimination of various noxious pollutants from the water system. Polyethyleneimine (PEI)-modified magnetic hydrogel nanocomposites (PEI-mHNCs) with three-dimensional networks were prepared based on poly (acrylamide-co-acrylic acid) and PEI-modified magnetic nanoparticle and used for the removal of crystal violet dye from aqueous solution. XRD results preliminarily confirmed the target structure of PEI-mHNCs without destroying the structure of magnetic nanoparticles during modification and radical polymerization. PEI-mHNCs had rough and uneven surface with many coarse porous and gap structure. PEI-mHNCs had crystal violet adsorption capacity of 198.5, 286.3 and 372.6 mg/g for initial dye concentration of 300, 500 and 700 mg/L, respectively. Dye absorption approached absorption equilibrium at 90 min and PEI-mHNCs had maximum dye absorption capacity at pH = 8. The adsorption isotherms and kinetics conformed to the Langmuir model and pseudo-second-order kinetic model, respectively. Thermodynamic studies revealed that crystal violet adsorption for PEI-mHNCs was a spontaneous, exothermal and decreased entropy process.Besides, PEI-mHNCs had good magnetic responsiveness, desorption and reusability which made it an efficient adsorbent for the removal of cationic dyes from an aqueous solution.

Keywords Polyethyleneimine · Hydrogel · Nanocomposites · Magnetic · Adsorption

✉ Tao Wan
wantaos@126.com

[1] State Key Lab of Geohazard Prevention and Geoenvironment Protection, Chengdu University of Technology, Chengdu 610059, Sichuan, China

[2] Mineral Resources Chemistry Key Laboratory of Sichuan Higher Education Institutions, Chengdu University of Technology, Chengdu 610059, Sichuan, China

Introduction

Wastewater effluents from different industries, such as textile, leather, paper, rubber, plastic, cosmetic, pharmaceutical and food, contain several kinds of synthetic dyestuffs [1–3]. The effluents are discarded into rivers and lakes, changing their biological life [4, 5]. Organic dyes are highly undesirable due to the highly intense colors and toxicities to human and other aquatic organisms even in low concentrations [6]. Crystal violet (CV) is a triarylmethane cationic dye widely used for purple coloration in textile industries for dying cotton and temporary hair colorant [7]. Besides, crystal violet is bacteriostatic agent for animal and veterinary medicine and used as dermatological agent for a biological strain in medical purpose [8].

It can cause harmful effects to the human body such as eye and skin irritation, heartbeat increase, cyanosis, and respiratory and kidney failure at extreme degree [9, 10]. Due to the obvious color fastness, resistance to microbial degradation and photolysis stability of most dyes, their effective removal in water has become a major challenge for traditional water treatment methods [11]. As a result, the development of innovative technologies for the effective removal of dyes from water has received considerable research attention [12].

Up to now, various chemical, physical and biological methods [13] were used for wastewater treatment including filtration, advanced oxidation, flocculation and coagulation, catalysis, photo and chemical degradation [14–16] and adsorption [17]. Among these methods, adsorption is the most appropriate and reasonable choice for the removal of organic pollutants and inorganic heavy metal ions from wastewater due to low cost and easy operation [18]. However, the adsorption technique has the disadvantage of being inconvenient in separating the absorbents from the aqueous solution.

In recent years, hydrogel polymers with three-dimensional networks and many functional groups such as amino, hydroxyl, carboxylic and sulfonic acid have been widely used in the dye removal from aqueous solutions because of their advantages such as high flexibility in the design of structures and properties, chemical stability in harsh environments, feasible regeneration and thermal durability [19–26]. For example, Pandey et al. [27] prepared hydrogels nanocomposite (HNC) by an aqueous free radical in situ crosslink copolymerization of acrylamide (AAm) and acrylic acid (AA) in aqueous solution of Karaya gum-stabilized Ag NPs. The removal efficiency of HNC was found to be 99% at pH 8 for a crystal violet (CV) after 1 h. The high CV removal efficiency is explained by H-bonding interactions, as well as dipole–dipole and electrostatic interactions between anionic adsorbent and cationic dye molecules. They synthesized LBG-cl-Poly (DMAAm) hydrogel via free radical in situ polymerization of *N*,*N*-dimethyl acrylamide and locust bean gum (LBG) by employing *N*,*N*′-methylene bis (acrylamide) as cross-linkers. Adsorption behavior of hydrogel was investigated for the adsorption of cationic dye-Brilliant green (BG) and it was found to have a maximum adsorption capacity of 142.85 mg. $g^{-1}$and BG removal of 97.7% in 50 mg.L^{-1} of dye solution [28].

However, the adsorption technique has the disadvantage of being inconvenient in separating the absorbent from the aqueous solution. The use of magnetic

nanoparticles is one of the improved methods [29–31]. Magnetic nanoparticles have attracted tremendous attention owing to their high specific surface area, low toxicity, biocompatibility and easy separation from wastewater by an external magnetic field [32]. Magnetic adsorbents are typically evenly distributed in polymer matrixes, and various magnetic adsorbents, such as magnetic chitosan particles [33], magnetic carbon nanotubes [34], magnetic graphene [35] and magnetic hydrogels [36, 37], have been developed for dye wastewater treatment.

Polyethylenimine (PEI) is a typical water-soluble polyamine and contains a great number of amine groups. The presence of nitrogen-containing groups on its molecular chains makes it easily be positively charged in a broad pH range, thus facilitating the adsorption of anionic dyes via strong electrostatic attraction [38–40]. Thus, combining functionalities of magnetism and hydrogel structures may show facile separation properties and highly efficient dye adsorption. Up to now, few literatures have been reported about the preparation and its cationic dye absorption behaviors of PEI-modified magnetic hydrogel nanocomposites based on poly (acrylamide-co-acrylic acid) and PEI-modified magnetic nanoparticles. We assumed the design of PEI-modified magnetic hydrogel nanocomposites (PEI-mHNCs) with three-dimensional networks would achieve the purpose of developing a novel adsorbent with high dye adsorption capability and facile separation property.

In this work, we synthesized PEI-mHNCs with three-dimensional networks based on poly (acrylamide-co-acrylic acid) and PEI-modified magnetic nanoparticles. Effect of parameters (i.e., pH value, adsorption time, initial dye concentration) on the adsorption capacity of crystal violet were investigated. The kinetic and isotherm of crystal violet adsorption process for PEI-mHNCs were analyzed. Desorption and reusability, as well as structure and morphologies of PEI-mHNCs, were also evaluated.

Materials and methods

Materials

Acrylic acid (AA), acrylamide (AM), ammonium persulfate (APS) and sodium bisulfite (SBS) were purchased from Chengdu Kelong Reagent Chemicals (China). $FeCl_3.6H_2O$, $FeCl_2.7H_2O$ and γ-chloropropyl trimethoxy silane (CTS) were purchased from Chengdu Huaxia Reagent Chemicals (China). Polyethylenimine (PEI) and polyethylene glycol diacrylate (PEGD) were purchased from Chengdu Aike Chemical Reagent (China). All chemicals used were of analytical reagent grade without further purification.

Preparation of magnetic nanoparticles (MNPs)

Magnetic nanoparticles (MNPs) were synthesized according to the known procedure by co-precipitation method [42–44]. Typically, 19.6 g $FeCl_3.6H_2O$) and 7.2 g $FeCl_2.7H_2O$ were dissolved in deionized water (300 mL) and stirred at

60 °C. Then, 2 mol/L of ammonia solution was added dropwise under vigorous stir until the pH reached 11 and the reaction mixture was stirred for 4.5 h. After cooling down to room temperature, the magnetic nanoparticles were separated by an external magnet and washed several times with deionized water. Finally, the magnetic nanoparticles were dried at 60 °C for 24 h under vacuum.

Preparation of CTS-modified magnetic nanoparticles (CTS-MNPs)

Typically, 1 g magnetic nanoparticles were dissolved in deionized water and ethanol (100 mL) with water/ethanol volume ratio of 1:1 and stirred at 50 °C under N_2 protection. Then, 1.5 mL 30% ammonia solution was added dropwise under vigorous stir, followed by slow addition of 3 mL silane coupling agent (CTS) under vigorous stirring. After 4 h reaction under N_2 protection, the temperature was cooled down to room temperature and CTS-modified magnetic nanoparticles were separated by an external magnet and washed several times with deionized water and ethanol alternately. Finally, CTS-modified magnetic nanoparticles (CTS-MNPs) were dried at 60 °C for 24 h under vacuum.

Preparation of PEI-modified magnetic nanoparticles (PEI-MNPs)

Typically, 1 g CTS-MNPs and1g PEI were dissolved in 100 mL deionized water and stirred at 50 °C for 5 h under N_2 protection. After cooling down to room temperature, PEI-modified magnetic nanoparticles (PEI-MNPs) were separated by an external magnet, washed several times with deionized water and ethanol alternately, and dried at 60 °C for 24 h under vacuum.

Preparation of PEI-modified magnetic hydrogel nanocomposites (PEI-mHNCs)

To prepare the PEI-modified magnetic hydrogel nanocomposites (PEI-mHNCs), 10 g acrylic acid, 10 g acrylamide and 3.61 g NaOH were dissolved in 100 mL deionized water and stirred for 45 min at room temperature. Then, 3.0 g PEI-MNPs and 0.15 g polyethylene glycol diacrylate were added into the above monomer solution and stirred for 30 min at room temperature. After that, the temperature was raised to 60 ℃, followed by the slow addition of 0.24 g ammonium persulfate and 0.077 g sodium bisulfite. The reaction mixture was stirred for 5 h at 60 ℃. After cooling down to room temperature, PEI-mHNCs were separated by an external magnet, washed several times with deionized water and ethanol alternately and left over night in ethanol. Finally, PEI-mHNCs were dried at 60 °C for 24 h under vacuum.

Dye adsorption experiment using batch methods

Batch adsorption experiments were carried out on a thermostatic shaker with a constant speed of 120 rpm at room temperature to study adsorption property of crystal violet for PEI-mHNCs. 0.1 g dry and milled PEI-mHNCs was immersed in 100 mL crystal violet solution with desired initial concentration and pH for a given time at different temperatures, and then crystal violet concentration left in the solution was analyzed by UV–visible spectrophotometer.

Dye absorption capacity was calculated using the following equation:

$$q_e = \left(C_0 - C_e\right)V/m \tag{1}$$

where q_e is the amount of dye adsorbed (mg/g), C_0 and C_e are initial and equilibrium concentration of dye (mg/L) in the testing solution, respectively. V is the volume of the dye solution (L) and m is the mass of dry PEI-mHNCs (g).

Desorption and regeneration experiments

Dye desorption was carried out in 0.5 M HCl solution (50 mL) for 90 min. After a given time, the supernatant was subjected to determine the dye concentration by UV–visible spectrophotometer and desorption percentage is calculated according to Eq. (2).

$$\text{Desorption} = M_d/M_0 \times 100\% \tag{2}$$

where M_0 is the amount of dye adsorbed by PEI-mHNCs and M_d is the amount of dye desorbed.

After dye desorption, PEI-mHNCs were removed from desorption solution using an external magnet, and washed with distilled water, dried at 60 °C for 24 h, and used for the subsequent runs. To test the reusability of PEI-mHNCs, this adsorption–desorption cycle was repeated five times using the same adsorbents.

Characterization of the magnetic hydrogel nanocomposites

Morphologies of MNPs, CTS-MNPs and PEI-MNPs were observed by JEM-100CX transmission electron microscopy (TEM). The samples were dropped onto a copper net sprayed with carbon, dried in vacuum, and then tested on a transmission electron microscope with an acceleration voltage of 100 kV. Micrographs of PEI-mHNCs were observed by HITACHI S-530 scanning electron microscope (SEM). Before SEM observation, all samples were fixed on aluminum stubs and coated with gold. X-ray diffraction analysis was carried out on DMX-IIIC diffractometer. Magnetic properties were determined by a LakeShore 7407 vibrating sample magnetometer (VSM) at room temperature.

Results and discussion

TEM and SEM characterization of the magnetic materials

Figure 1a–c shows the TEM images of MNPs, CTS-MNPs and PEI-MNPs, respectively. It is obviously that MNPs, CTS-MNPs and PEI-MNPs have average size of 15–20 nm with irregular particle shape and partial agglomeration phenomenon. This may be related to the high vacuum drying process of TEM, during which magnetic nanoparticles are easy to agglomerate. After surface modification with CTS and PEI, the agglomeration of magnetic nanoparticles is reduced due to the steric effect of organic molecular chains grafted on the surface of magnetic nanoparticles [45]. Besides, the above TEM results signify that unmodified and modified magnetic Fe_3O_4 particles with nanometer size are successfully prepared. As can be seen from Fig. 1d, the surface of PEI-mHNCs is rough and uneven with many coarse porous and gap structure. Such a structure can help crystal violet rapidly infiltrate and diffuse into the three-dimensional network of magnetic polymer adsorbent, which can enhance the crystal violet adsorption for PEI-mHNCs.

XRD analysis of the magnetic materials

Figure 2 demonstrates the XRD curves of MNPs, CTS-MNPs, PEI-MNPs and PEI-mHNCs, respectively. As can be seen from XRD spectra, the sharp characteristic diffraction peaks of MNPs, CTS-MNPs and PEI-MNPs appear at $2\theta = 0.23°$, 35.50°, 43.36°, 53.67°, 57.12° and 62.72°, which correspond to the (220), (311),

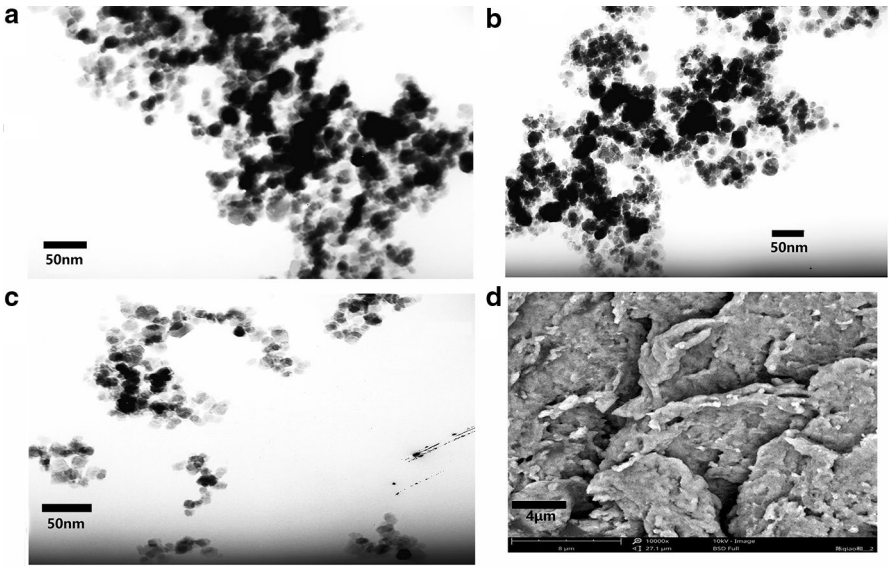

Fig. 1 TEM images of MNPs (**a**), CTS-MNPs (**b**) and PEI-MNPs (**c**). SEM image of PEI-mHNCs (**d**)

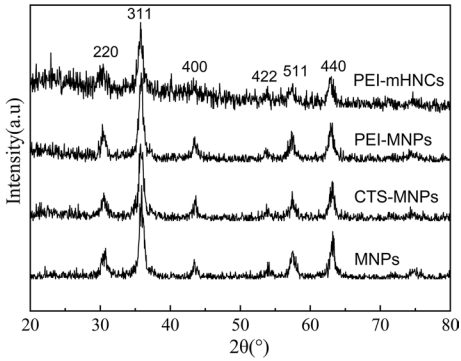

Fig. 2 XRD spectra of MNPs, CTS-MNPs, PEI—MNPs and PEI-mHNCs

(400), (422), (511) and (440) crystal faces of Fe_3O_4 cubic phase, respectively. These results are consistent with the characteristic diffraction peaks of standard Fe_3O_4 (JCPDS No. 19–06290) [46]. Meanwhile, the diffraction spectra of MNPs, CTS-MNPs and PEI-MNPs have no impurity peaks, indicating that the obtained MNPs, CTS-MNPs and PEI-MNPs have high purity and good crystallinity. Crystalline structure of Fe_3O_4 is not affected after surface modification. It is worth noting that PEI-mHNCs has characteristic diffraction peaks of standard magnetic Fe_3O_4 appearing at $2\theta = 30.23°$, 35.50°, 57.12° and 62.72°, indicating that the crystal structure of magnetic Fe_3O_4 is not destroyed during the radical copolymerization of acrylamide and acrylic acid.

Magnetic property of the magnetic materials

VSM was employed to study the magnetic behaviors of MNPs, CTS-MNPs, PEI-MNPs and PEI-mHNCs at room temperature, as shown in Fig. 3. The hysteresis loops of all samples showed negligible coercivity and remanence at room temperature, indicating the superparamagnetic nature of MNPs, CTS-MNPs, PEI-MNPs and PEI-mHNCs [47]. Saturation magnetization of magnetic nanoparticles prepared by the co-precipitation method reached 67.76 emu/g. At the same time, the saturation

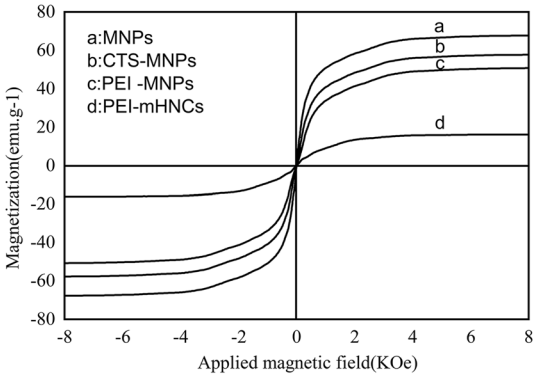

Fig. 3 Magnetization curves of MNPs, CTS-MNPs, PEI-MNPs and PEI-mHNCs

magnetization of magnetic nanoparticles modified with CTS and PEI decreased slightly with the saturation magnetization of 58.12 emu/g and 51.03 emu/g, respectively. Although the saturation magnetization decreased to 16.47 emu/g for PEI-mHNCs due to none-magnetic response of silane coupling agent and the polymer matrix, PEI-mHNCs still have a certain magnetic response. Therefore, PEI-mHNCs can facilitate solid–liquid separation with the advantages of high separation efficiency, time and labor saving and no secondary pollution under an external magnetic field.

Effect of pH on dye adsorption properties of PEI-mHNCs

pH value is an important parameter that can competently impact the dye adsorption potential onto adsorbents [48, 49]. The adsorption condition was as follows: adsorbent dosage of 1 g/L, temperature of 25 ℃, initial concentration of 700 mg/L for crystal violet and contact time at 90 min. As shown in Fig. 4a, the adsorption capacity of crystal violet for PEI-mHNCs increased with the increase of pH value. However, the adsorption capacity of crystal violet of PEI-mHNCs decreased slowly when the pH exceeded 8. When the pH is low, H^+ within the polymeric network can compete with the cationic groups of crystal violet, which make it difficult for crystal violet to be absorbed by electrostatic attraction with the functional groups of PEI-mHNCs. In addition, PEI has many amino and imine groups. These groups are easy to proton into ammonium cations which have the electrostatic repulsion force with cationic groups of crystal violet in the condition of low pH value. Hence, adsorption capacity of crystal violet for PEI-mHNCs decreases. With the increase of pH value, the carboxyl group of PEI-mHNCs can ionize to produce carboxyl anion, which increases the electrostatic repulsive force of magnetic polymeric chains and is in favor of the extension and expansion of polymer network. Besides, the amino protonation of PEI chains decreases with increasing pH value. Therefore, PEI-mHNCs have more amino and imine groups which can absorb crystal violet vis hydrogen bond and increases the adsorption capacity of crystal violet. However, when pH is higher than 8, the concentration of Na^+ in the polymer network is high, increasing the shielding effect of Na^+ on the carboxylic groups of polymer molecular chain, reducing the electrostatic repulsive force of macromolecular chains, and making three-dimensional network difficult for expansion. As a result, dye adsorption capacity of PEI-mHNCs is reduced.

Effect of initial dye concentration on dye adsorption properties of PEI-mHNCs

The influence of initial dye concentration on the adsorption capacity of crystal violet for PEI-mHNCs is shown in Fig. 4b. The adsorption condition was as follows: adsorbent dosage of 1 g/L, temperature of 25 ℃, pH value of 8, and contact time at 90 min. Obviously with the increase of initial dye concentration, the adsorption capacity of crystal violet for PEI-mHNCs increases rapidly at first and then

increases slowly. PEI-mHNCs has crystal violet adsorption capacity of 198.5 mg/g, 286.3 mg/g and 372.6 mg/g for initial dye concentration of 300 mg/L, 500 mg/L and 700 mg/L, respectively.

In general, the increase of adsorption capacity caused by the increase of initial concentration is mainly attributed to the driving force generated by the concentration difference between the solid–liquid interface [50]. When dye concentration is low, PEI-mHNCs has a large number of active and exposed adsorption centers which are not occupied by dye molecule, resulting in a rapid increasing adsorption capacity. With the increase of initial dye concentration, concentration gradient for dye in solution and PEI-mHNCs increases continuously, upgrading the mass transfer driving force, making more dye diffuse and permeate into the polymeric networks. On the other hand, with the increasing dye concentration, many adsorption centers for PEI-mHNCs are occupied by dye molecules, resulting in limited and decreased adsorption vacancies for PEI-mHNCs. As a consequence, dye adsorption capacity for PEI-mHNCs increases slowly [51].

Effect of adsorption time on dye adsorption properties of PEI-mHNCs

Adsorption time is an important variable to design an economical adsorbent for the wastewater effluents. The adsorption condition was as follows: adsorbent dosage of 1 g/L, temperature of 25 ℃, pH value of 8 and initial concentration of 500 mg/L for crystal violet. As can be seen from Fig. 4c, dye adsorption rate for PEI-mHNCs is relatively fast at the initial stage of adsorption. With the extension of adsorption time, dye adsorption rate slows down, and gradually approaches the absorption equilibrium at 90min, indicating that PEI-mHNCs has a high adsorption rate for cationic crystal violet.

At the initial stage of adsorption, there are many adsorption vacancies on the surface of PEI-mHNCs, so there is a large concentration gradient of dye in the aqueous solution and on the surface of PEI-mHNCs, leading to a rapid dye adsorption rate in the initial stage of adsorption. With the extension of adsorption time, cationic crystal violet gradually fills up the adsorption vacancies on the surface of PEI-mHNCs and begins to enter the polymeric networks. Dye adsorption rate slows down because of the resistance to enter the pores inside the polymeric networks and the slow mass transfer rate. When the adsorption vacancies on the surface and inside of the polymeric networks are both occupied by cationic crystal violet, dye adsorption tends to balance, and dye adsorption of PEI-mHNCs reaches adsorption equilibrium.

Dye adsorption kinetics for PEI-mHNCs

To investigate the dye adsorption kinetics for PEI-mHNCs, pseudo-first-order [52] and pseudo-second-order equations [53] were used to test the experimental data of adsorption of crystal violet for PEI-mHNCs.

The pseudo-first-order rate expression of Lagergren is given as:

$$\ln(q_e - q_t) = \ln q_e - k_1 t \quad (3)$$

The pseudo-second-order kinetic model is expressed as:

$$t/q_t = 1/\left(k_2 q_e^2\right) + t/q_e \quad (4)$$

where q_e is the amount of adsorbed dye onto PEI-mHNCs at equilibrium (mg/g), q_t is the amount of dye adsorbed at time t (mg/g), k_1 and k_2 are the first order rate constant and second order rate constant, respectively.

A straight line of ln $(q_e - q_t)$ versus t suggests the applicability of pseudo-first-order kinetic model to fit the experimental data, whereas a linear relationship between t/q_t versus t indicates pseudo-second-order kinetic model. The slopes and intercepts of plots of ln $(q_e - q_t)$ versus t and the slopes and intercepts of plots of t/q_t against t are used to determine the first-order rate constant k_1 and equilibrium adsorption q_e, as well as the second-order rate constant k_2 and equilibrium adsorption q_e, respectively.

Dye adsorption kinetics parameters for PEI-mHNCs are shown Table 1. The correlation coefficients (R^2) for the pseudo-first-order kinetic model are low ($R^2 < 0.85$) for crystal violet absorption with different dye initial concentrations. Also, the calculated q_e values (32.7, 52.5 and 98.8 mg/g) obtained from the pseudo-first-order kinetic model do not give reasonable values, which are much lower than experimental values (196.5, 282.8 and 372.6 mg/g). This suggests that the adsorption of crystal violet of PEI-mHNCs is not a pseudo-first-order process. However, the correlation coefficients for the pseudo-second-order kinetic model are very close to 1 ($R^2 > 0.99$), and the calculated q_e values almost agree with the experimental data. These results indicate that the crystal violet adsorption of PEI-mHNCs belongs to the second-order kinetic model.

Isothermal dye adsorption for PEI-mHNCss

Langmuir and Freundlich adsorption isotherm models were used to determine the appropriate isotherm of crystal violet adsorption for PEI-mHNCs. The linearized form of Langmuir adsorption isotherm is expressed in Eq. (5).

$$1/q_e = 1/\left(K_L q_m C_e\right) + 1/q_m \quad (5)$$

In Eq. (5), C_e is the equilibrium concentration of dye in solution (mg/L), q_e is the equilibrium concentration of dye for the adsorbent (mg/g), q_m is the monolayer

Table 1 Kinetic information calculated from crystal violet absorption by PEI-mHNCs

Conc/mg/L	Pseudo-first-order				Pseudo-second-order		
	q_e/mg/g	k_1/1/min	R^2	q_{exp}/mg/g	q_e/mg/g	k_2/g/mg/min	R^2
300	32.7	0.028	0.8457	196.5	197.9	0.0021	0.9965
500	52.5	0.022	0.8317	282.8	285.7	0.0016	0.9972
700	98.8	0.019	0.8389	372.6	373.1	0.0012	0.9937

adsorption capacity of the adsorbent (mg/g) and K_L (L/mg) is the Langmuir equilibrium constant. The values of q_m and K_L are determined from the slope and intercept of the plots of $1/q_e$ versus C_e.

The linearized Freundlich isotherm has the general form given in Eq. (6).

$$\ln q_e = \ln K_F + (1/n)\ln C_e \tag{6}$$

In Eq. (6), q_e is the amount of dye adsorbed at equilibrium (mg/g), C_e is the equilibrium concentration of dye in solution (mg/L), K_F and n are the Freundlich constants, indicating adsorption capacity and adsorption intensity, respectively. The values of n and K_F are calculated from slope and intercept of plots of $\ln q_e$ versus $\ln C_e$.

The values of the Langmuir and Freundlich constants Q_m, K_L, K_F, n and the correlation coefficients (R^2) are listed in Table 2. The correlation coefficients ($R^2 > 0.99$) of Langmuir adsorption models for crystal violet by PEI-mHNCs are higher than those of Freundlich adsorption models (($R^2 < 0.93$). Besides, the adsorption capacities of crystal violet calculated by Langmuir fitting equation are in good agreement with the experimental data. The results indicate that the adsorption process of crystal violet for PEI-mHNCs is consistent with Langmuir adsorption model with monolayer adsorption.

Thermodynamic of dye adsorption by PEI-mHNCs

To further investigate the dye adsorption process, the experimental data under different temperatures varying from 298 to 338 *K* were analyzed by Eqs. (7) , (8) and (9) to obtain the thermodynamic parameters including the Gibbs free energy (ΔG^{Θ}), enthalpy (ΔH^{Θ}) and entropy (ΔS^{Θ}).

$$\Delta G^{\Theta} = -RT\ln K_d = -RT\ln\left(q_e/C_e\right) \tag{7}$$

$$\Delta G^{\Theta} = \Delta H^{\Theta} - T\Delta S^{\Theta} \tag{8}$$

$$\ln\left(q_e/C_e\right) = \Delta S^{\Theta}/R - \Delta H^{\Theta}/(RT) \tag{9}$$

Table 2 Langmuir and Freundlich isotherm constants for adsorption isotherm curve fitting parameters of crystal violet adsorption by PEI-mHNCs with dye initial concentration of 900 mg/L

T/*k*	Langmuir				Freundlich		
	q_m/mg/g	K_L/L/mg	R^2	q_{exp}/mg/g	*n*	K_F	R^2
298	474.4	0.0051	0.9929	473.1	1.1476	7.8365	0.9189
308	468.3	0.0053	0.9935	461.5	1.1534	7.8587	0.9211
318	462.6	0.0052	0.9937	446.8	1.1526	7.9878	0.9205
328	455.7	0.0054	0.9928	437.6	1.1517	7.7624	0.9199
338	445.9	0.0052	0.9941	424.4	1.1498	7.8512	0.9231

Table 3 Thermodynamic parameters of crystal violet adsorption for PEI-mHNCs

Thermodynamic parameters	T (K)				
	298	308	318	328	338
ΔH^{Θ} (kJ/mol)	–3.57				
ΔS^{Θ} (J/mol.K^{-1})	–2.28				
ΔG^{Θ} (kJ/mol)	–2.89	–2.86	–2.84	–2.82	–2.79

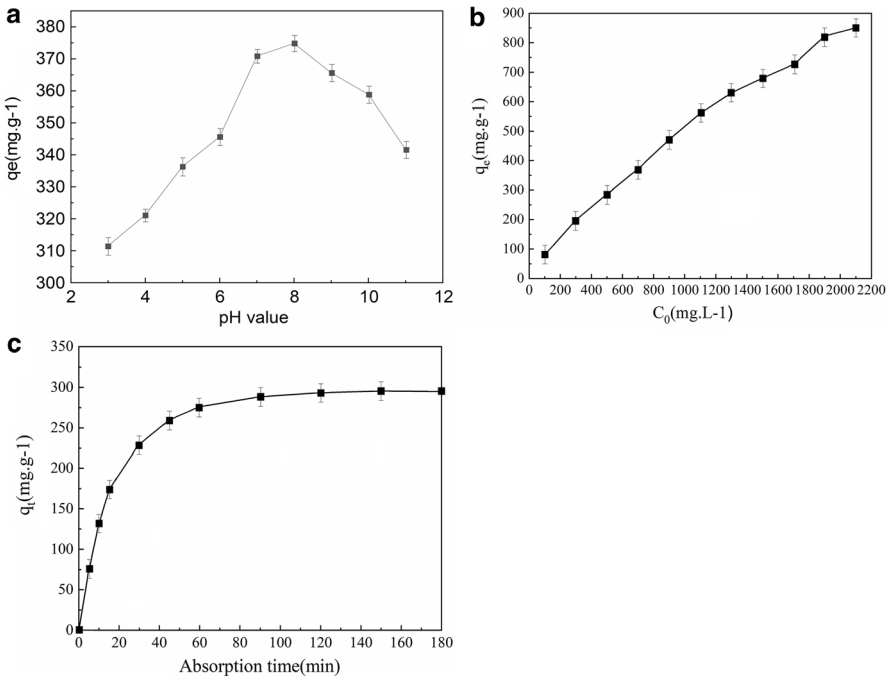

Fig. 4 Effects of pH (**a**); effects of initial concentration of crystal violet (**b**); effects of adsorption time **c** on crystal violet adsorption capacity for PEI-mHNCs

where R (8.314 J.mol^{-1}. K^{-1}) is the gas constant, T is the temperature in K and K_d is the equilibrium constant which can be calculated from q_e/C_e.

Adsorption thermodynamic parameters such as ΔG^{Θ}, ΔH^{Θ} and ΔS^{Θ} can be obtained based on ln $(q_e/C_e) \sim 1/T$ curve and the results were shown in Table 3. Obviously with the increase of adsorption temperatures, dye adsorption capacity of PEI-mHNCs gradually decreases. The negative values of ΔG^{Θ} at different temperatures indicate dye adsorption is thermodynamically spontaneous process. The absolute values of ΔG^{Θ} gradually decrease as the temperature increases, implying that lower temperature facilitates the adsorption of dyes. The negative values of ΔH^{Θ} and ΔS^{Θ} confirm that the dye adsorption process for PEI-mHNCs is an exothermal and decreased entropy process.

Desorption-regeneration performance of PEI-mHNCs

It is well known that the recyclability and stability of the adsorbent is crucial for practical applications. After dye desorption by HCl solution, PEI-mHNCs were removed from desorption solution using an external magnet, and washed with distilled water, dried at 60 °C for 24 h, and used for the subsequent runs. Figure 5a shows the desorption curves of PEI-mHNCs using hydrochloric acid as desorbent. Dye desorption of PEI-mHNCs gradually decreased after five cycles of recycling, but the reduction was not significant. After five cycles of recycling, dye desorption of PEI-mHNCs was still higher than 93%, indicating that PEI-mHNCs had good dye desorption performance. As indicated in Fig. 5b, after five cycles, PEI-mHNCs had crystal violet absorption capacity of 268 mg/g which reached 89.9% of that (298 mg/g) for the first absorption, indicating good reversibility and recyclability of PEI-mHNCs. The decrease of dye adsorption capacity may be caused by a few active sites not being released or incomplete dye desorption.

Comparison of adsorption capacity with other hydrogel adsorbents

In recent years, extensive research has been done all over the world to find an adsorbent with a low economic cost, easy processability, and high adsorption capacity. To evaluate the CV adsorption of PEI-mHNCs, CV adsorption capacity of PEI-mHNCs was compared with other hydrogel adsorbents (Table 4). The results showed that PEI-mHNCs had good CV adsorption capacity, which was higher than most of the other hydrogel adsorbents in the literature. Besides, PEI-mHNCs had good magnetic responsiveness, desorption and reusability which made it an efficient adsorbent for the removal of cationic dyes from an aqueous solution.

Given the chemical structure of the cationic crystal violet dye and PEI-mHNCs, a possible mechanism for the interactions between PEI-mHNCs and cationic crystal violet dye is illustrated in Scheme 1. PEI-mHNCs has many functional groups such as NH_2, COOH, COONa and $CONH_2$, which can interact with the cationic crystal violet dye via H- bonding and electrostatic force between the positively charged dye molecules and negatively charged PEI-mHNCs. Besides, PEI-mHNCs has rough

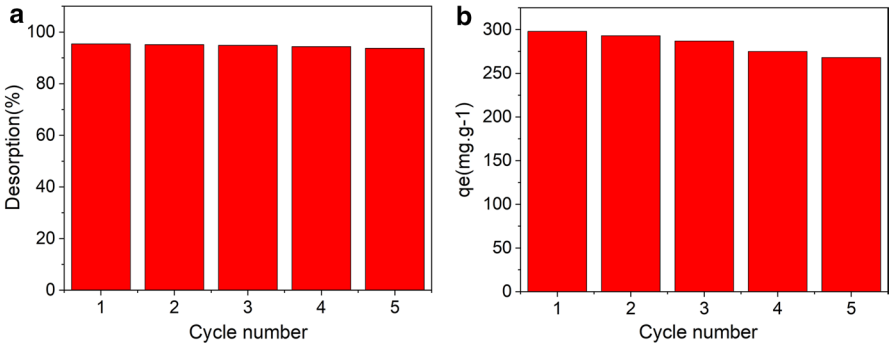

Fig. 5 Desorption (**a**) and recycling performance (**b**) for PEI-mHNCs toward crystal violet

Table 4 Comparison of adsorption capacity of PEI-mHNCs for CV dye removal with other hydrogel absorbents

Absorbents	Conditions	Q_{max} (mg.g^{-1})	References
Poly (acrylic acid-acrylamide- methacrylate) and amylose	pH 7.4/298 K	35	[19]
Acrylamide/graphene oxide bonded sodium alginate (AM-GO-SA) HNC	pH 8/303 K	100.3	[20]
Polysaccharide-based magnetic nanocomposite	pH 7/298 K	80.64	[21]
Hybrid adsorbents of tannin and APTES	pH 2/323 K	349.4	[22]
Surfactant-modified magnetic nanoadsorbent	pH 6	247.7	[30]
KG-cl-P (AAm-co-AN) @AgNPs HNC	pH 8/298 K	1000	[28]
Polyacrylic acid-bound magnetic nanoparticles	pH 6/298 K	116	[29]
Magnetic nanocomposite	pH 8.5/303 K	111.80	[31]
β-cyclodextrin-biogenic Fe (0) nanoadsorbents	pH 9	293	[54]
Functionalized carboxymethyl cellulose microbeads	pH 8/303 K	107.52	[26]
Poly (acrylamide)-kaolin composite hydrogel	pH 10/308 K	23.8	[25]
P (AAm-MA)/MMT	pH 7/293 K	20.36	[24]
Magnetized orange peel	pH 8/298 K	555.55	[23]
PEI-mHNCs	pH 8/298 K	372.6	This work

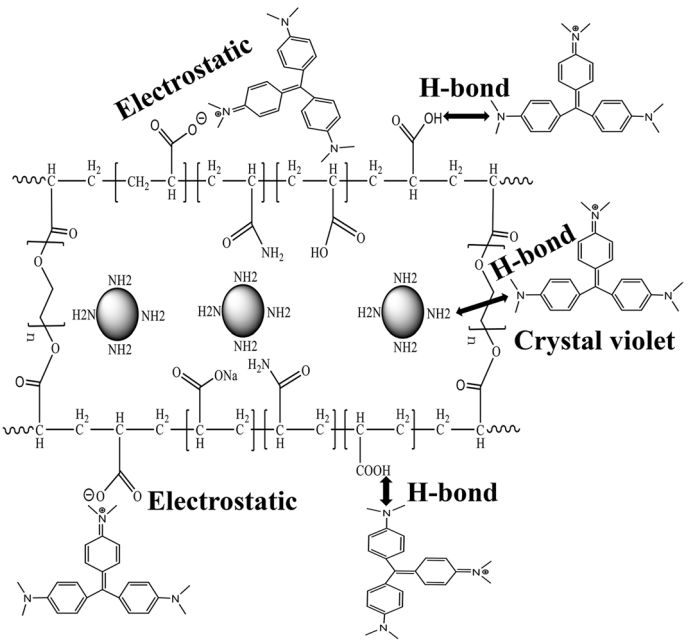

Scheme 1 Possible interactions between PEI-mHNCs and cationic crystal violet dye

and porous structure, which can promote crystal violet to infiltrate into the three-dimensional network of magnetic polymer adsorbent, and thus enhance the crystal violet adsorption for PEI-mHNCs.

Conclusion

PEI-modified magnetic hydrogel nanocomposites (PEI-mHNCs) with three-dimensional networks were prepared by copolymerization of acrylamide and acrylic acid in the presence of PEI-modified magnetic nanoparticles. XRD results show that PEI-mHNCs have been successfully prepared without destroying high crystallinity of magnetic Fe_3O_4. PEI-mHNCs absorbed crystal violet rapidly and approached absorption equilibrium at 90 min. Dye adsorption capacity of PEI-mHNCs increased with the increase of initial dye concentration and the increase of pH to 8. The adsorption isotherms and kinetics were in agreement with the Langmuir equation and pseudo-second-order kinetic equation, respectively. Crystal violet adsorption for PEI-mHNCs is a spontaneous, exothermal and entropy reduction process. In addition, PEI-mHNCs had good magnetic separation, desorption and recycling, making it potential applications in removing cationic dye from the aqueous solution.

Acknowledgements This work was supported by the Key Research and Development Program of Sichuan province (Grant No. 2019YFG0264); Technology Foundation for Selected Overseas Chinese Scholar, Department of Personnel of Sichuan province (Grant No. 19BZ08-009); State Key Laboratory of Geohazard Prevention and Geoenvironment Protection (Grant No. SKLGP2018Z005).

References

1. Chiou MS, Ho PY, Li HY (2004) Adsorption of anionic dyes in acid solutions using chemically cross-linked chitosan beads. Dyes Pigments 60:69–84
2. Zhang F, Ma B, Jiang X, Ji Y (2016) Dual function magnetic hydroxyapatite nanopowder for removal of malachite green and Congo red from aqueous solution. Powder Technol 302:207–214
3. Chen B, Liu Y, Chen S, Zhao X, Yue W, Pan X (2016) Nitrogen-rich core/shell magnetic nanostructures for selective adsorption and separation of anionic dyes from aqueous solution. Environ Sci Nano 3:670–681
4. Walker GM, Hansen L, Hanna JA, Allen SJ (2003) Kinetics of a reactive dye adsorption onto dolomitic sorbents. Water Res 37:2081–2089
5. Stydin M, Dimitris IK, Verykios XE (2004) Visible light-induced photocatalytic degradation of acid orange 7 in aqueous TiO2 suspensions. Appl Catal Environ 47:189–193
6. Zhu H, Jiang R, Xiao L, Chang Y, Guan Y, Li X, Zeng G (2009) Photocatalytic decolorization and degradation of Congo Red on innovative crosslinked chitosan/nano-CdS composite catalyst under visible light irradiation. J Hazard Mater 169:933–940
7. Gupta R, Pandit C, Pandey S (2022) Potential and future prospects of biochar-based materials and their applications in removal of organic contaminants from industrial wastewater. J Mater Cycles Waste 24:852–876
8. Puri C, Sumana G (2018) Highly effective adsorption of crystal violet dye from contaminated water using graphene oxide intercalated montmorillonite nanocomposite. Appl Clay Sci 166:102–112
9. Sarma GK, Sen Gupta S, Bhattacharyya KG (2016) Adsorption of Crystal violet on raw and acid-treated montmorillonite, K10, in aqueous suspension. J Environ Manage 171:1–10
10. Saeed A, Sharif M, Iqbal M (2010) Application potential of grapefruit peel as dye sorbent: Kinetics, equilibrium and mechanism of crystal violet adsorption. J Hazard Mater 179:564–572

11. Ahmad A, Khan N, Giri BS, Chowdhary P, Chaturvedi P (2020) Removal of methylene blue dye using rice husk, cow dung and sludge biochar: Characterization, application, and kinetic studies. Bioresour. Technol 123202.
12. Naseem K, Farooqi ZH, Begum R, Irfan A (2018) Removal of Congo red dye from aqueous medium by its catalytic reduction using sodium borohydride in the presence of various inorganic nano-catalysts: a review. J Clean Prod 187:296–307
13. Khapre M, Shekhawata A, Saravanan D, Pandey S, Jugade R (2022) Mesoporous Fe–Al-doped cellulose for the efficient removal of reactive dyes. Mater Adv 3:3278–3285
14. Bharathi D, Nandagopal JGT, Rajamani R, Pandit S, Kumar D, Pant B, Pandey S, Gupta PK (2022) Enhanced photocatalytic activity of St-ZnO nanorods for methylene blue dye degradation. Mater Lett 311:131637
15. Vinayagam R (2021) Green synthesis of magnetic α–Fe2O3 nanospheres using Bridelia retusa leaf extract for Fenton-like degradation of crystal violet dye. Appl Nanosci 11(8):2227–2234
16. Pandey S, Yeon Do JY, Kim J, Kang M (2020) Fast and highly efficient catalytic degradation of dyes using κ-carrageenan stabilized silver nanoparticles nanocatalyst. Carbohyd Polym 230:115597
17. Choi MY, Theerthagiri J, Jagannathan M, Maia G (2022) Surface tuning and interface engineering of advanced materials for detection and removal of toxic pollutants from industrial wastewater. Environ Res 210:112950
18. Pandey S, Fosso-Kankeu E, Spiro MJ, Waanders F, Kumar N, Ray SS, Kim J, Kang M (2021) Equilibrium, kinetic, and thermodynamic studies of lead ion adsorption from mine wastewater onto MoS2-clinoptilolite composite. Mater Today Chem 18:100376
19. Li S (2010) Removal of crystal violet from aqueous solution by sorption into semi-interpenetrated networks hydrogels constituted of poly (acrylic acid-acrylamide-methacrylate) and amylose. Bioresour Technol 101(7):2197–2202
20. Pashaei-Fakhri SJ, Peighambardoust R, Foroutan N, Arsalani B, Ramavandi, (2021) Crystal violet dye sorption over acrylamide/graphene oxide bonded sodium alginate nanocomposite hydrogel. Chemosphere 270:129419
21. Pourjavadi A, Hosseini SH, Seid FI, Soleyman R (2013) Magnetic removal of crystal violet from aqueous solutions using polysaccharide-based magnetic nanocomposite hydrogels. Polym Int 62:1038–1044
22. Leite AJB, Lima EC, Dos Reis GS, Thue PS, Saucier C, Rodembusch FS, Dias SLP, Umpierres CS, Dotto GL (2017) Hybrid adsorbents of tannin and APTES (3-aminopropyltriethoxysilane) and their application for the highly efficient removal of acid red 1 dye from aqueous solutions. J Environ Chem Eng 5:4307–4431
23. Ahmed M, Mashkoor F, Nasar A (2020) Development, characterization, and utilization of magnetized orange peel waste as a novel adsorbent for the confiscation of crystal violet dye from aqueous solution. Groundw Sustain Dev 10:100322
24. Aref L, Navarchian AH, Dadkhah D (2017) Adsorption of crystal violet dye from aqueous solution by poly (acrylamide-co-maleic acid)/montmorillonite nanocomposite. J Polym Environ 25:628–639
25. Shirsath S, Patil A, Bhanvase B, Sonawane S (2015) Ultrasonically prepared poly (acrylamide)-kaolin composite hydrogel for removal of crystal violet dye from wastewater. J Environ Chem Eng 3:1152–1162
26. OmerAM EGS, El-Subruit GM, Khalifa RE, Eltaweil AS (2020) Fabrication of novel iminodiacetic acid-functionalized carboxymethyl cellulose microbeads for efficient removal of cationic crystal violet dye from aqueous solutions. Int J Biol Macromol 148:1072–1083
27. Pandey S, Son N, Kang M (2022) Synergistic sorption performance of karaya gum crosslink poly (acrylamide-co-acrylonitrile) @ metal nanoparticle for organic pollutants. Int J Biol Macromol 210:300–314
28. Pandey S, Do JY, Kim J, Kang M (2020) Fast and highly efficient removal of dye from aqueous solution using natural locust bean gum based hydrogels as adsorbent. Int J Biol Macromol 143:60–75
29. Liao MH, Wu KY, Chen DH (2004) Fast Adsorption of Crystal Violet on Polyacrylic Acid-Bound Magnetic Nanoparticles. Sep Sci Technol 39(7):1563–1575
30. Muthukumaran C, Sivakumar VM, Thirumarimurugan M (2016) Adsorption isotherms and kinetic studies of crystal violet dye removal from aqueous solution using surfactant modified magnetic nanoadsorbent. J Taiwan Inst Chem Eng 63:354–362

31. Singh K, Gupta S, Singh AK, Sinha S (2011) Optimizing adsorption of crystal violet dye from water by magnetic nanocomposite using response surface modeling approach. J Hazard Mater 186:1462–1473
32. Reddy DHK, Yun YS (2016) Spinel ferrite magnetic adsorbents: Alternative future materials for water purification. Coordin Chem Rev 315:90–111
33. Oliveira LCA, Rios RVRA, Fabris JD, Sapag K, Gargc VK, Lago RM (2003) Clay-iron oxide magnetic composites for the adsorption of contaminants in water. Appl Clay Sci 22:169–177
34. Cho DW, Jeon BH, Chon CM, Schwartz FW, Jeong Y, Song H (2015) Magnetic chitosan composite for adsorption of cationic and anionic dyes in aqueous solution. J Ind Eng Chem 28:60–66
35. Madrakian T, Afkhami A, Ahmadi M, Bagheri H (2011) Removal of some cationic dyes from aqueous solutions using magnetic-modified multi-walled carbon nanotubes. J Hazard Mater 196:109–114
36. Yao Y, Miao S, Liu S, Ma LP, Sun H, Wang S (2012) Synthesis, characterization, and adsorption properties of magnetic Fe3O4@graphene nanocomposite. Chem Eng J 184:326–332
37. Mahdavinia GR, Mousanezhad S, Hosseinzadeh H, Darvish F, Sabzi M (2016) Magnetic hydrogel beads based on PVA/sodium alginate/laponite RD and studying their BSA adsorption. Carbohyd Polym 147:379–391
38. Zhang C, Dai YK, Wu YQ, Lu GW, Cao Z, Cheng JF, Wang KL, Yang HC, Xia YP, Wen XQ, Ma WZ, Liu CL, Zhaoli Wang ZL (2020) Facile preparation of polyacrylamide/chitosan/Fe3O4 composite hydrogels for effective removal of methylene blue from aqueous solution. Carbohyd Polym 234:115882
39. Guo DM, An QD, Li R, Xiao ZY, Zhai SR (2018) Ultrahigh selective and efficient removal of anionic dyes by recyclable polyethylenimine-modified cellulose aerogels in batch and fixed-bed systems. Colloid Surface A 555:150–160
40. Zhu WJ, Liu L, Liao Q, Chen X, Qian ZQ, Shen JY, Liang JL, Yao JM (2016) Functionalization of cellulose with hyperbranched polyethylenimine for selective dye adsorption and separation. Cellulose 23:3785–3797
41. Liang SW, Tang JY, Yao S, Zhu WX (2019) Removal characteristics of two anionic dyes by a polyethylenimine/poly (N, N-dimethylaminoethyl methacrylate) gel. RSC Adv 9:22907–22920
42. Kumar PS, Senthamara C, Durgadevi A (2014) Adsorption kinetics, mechanism, isotherm, and thermodynamic analysis of copper ions onto the surface modified agricultural waste. Environ Prog Sustain Energy 33:28–37
43. Kumar VV, Sivanesan S, Cabana H (2014) Magnetic cross-linked laccase aggregates—bioremediation tool for decolorization of distinct classes of recalcitrant dyes. Sci Total Environ 487:830–839
44. Paripoorani KS, Ashwin G, Vengatpriya P, Ranjitha V, Rupasree S, Kumar VV (2015) Insolubilisation of inulinase on magnetite chitosan micro-particles, an easily recoverable and reusable support. J Mol Catal B Enzym 113:47–55
45. DingY LF, Jiang Q, Du B, Sun H (2013) 12-Hydrothermal Synthesis and Characterization of Fe3O4 Nanorods. J Inorg Organomet Polym 23:379–384
46. Sun SH, Zeng H, Robinson DB, Raoux S, Rice PM, Wang SX, et al. Monodisperse MFe2O4 (M = Fe Co, Mn) nanoparticles (2004) J Am Chem Soc 126:273–279.
47. Liu D, Wu W, Ling J, Wen S, Gu N, Zhang X (2011) Effective PEGylation of iron oxide nanoparticles for high performance in vivo cancer imaging. Adv Funct Mater 21:1498–1504
48. Makhado E, Pandey S, Ramontja J (2019) Microwave-assisted green synthesis of xanthan gum grafted diethylamino ethyl methacrylate: An efficient adsorption of hexavalent chromium. Carbohyd Polym 222:114989
49. Doan VD, Tran TKN, Nguyen AT, Tran VA, Nguyen TD, Le VT (2021) Comparative study on adsorption of cationic and anionic dyes by nanomagnetite supported on biochar derived from Eichhornia crassipes and Phragmites australis stems. Environmental Nanotechnology, Monitoring & Management 16:100569
50. Zhang Y, Wang PL, Hussain Z, Zhang H, Wang HT, Chang N, Li F (2022) Modification and characterization of hydrogel beads and its used as environmentally friendly adsorbent for the removal of reactive dyes. J Clean Prod 342:130789
51. Saxena M, Lochab A, Saxena R (2021) Asparagine functionalized MWCNTs for adsorptive removal of hazardous cationic dyes: Exploring kinetics, isotherm and mechanism. Surf Interfaces 25:101187

52. Lagergren S (1898) About the theory of so-called adsorption of soluble substances. Kung Sven Veten Hand 24:1–39
53. McKay G, Ho YS (1998) The sorption of lead (II) on peat. Water Res 33:578–584
54. NasiriJ ME, Naghavi MR, Ghafoori M (2019) Removal of crystal violet from water using β-cyclodextrin functionalized biogenic zero-valent iron nanoadsorbents synthesized via aqueous root extracts of Ferula persica. J Hazard Mater 367:325–338